



Spectral light-reflection data dimensionality reduction for timely detection of yellow rust

Ran Aharoni¹ · Valentyna Klymiuk^{2,3} · Benny Sarusi^{1,4} · Sierra Young⁵ · Tzion Fahima^{2,3} · Barak Fishbain⁶ · Shai Kendler^{1,6}

Published online: 11 August 2020

© Springer Science+Business Media, LLC, part of Springer Nature 2020

Abstract

Yellow rust (YR) wheat disease is one of the major threats to worldwide wheat production, and it often spreads rapidly to new and unexpected geographic locations. To cope with this threat, integrated pathogen management strategies combine disease-resistant plants, sensors monitoring technologies, and fungicides either preventively or curatively, which come with their associated monetary and environmental costs. This work presents a methodology for timely detection of YR that cuts down on hardware and computational requirements. It enables frequent detailed monitoring of the spread of YR, hence providing the opportunity to better target mitigation efforts which is critical for successful integrated disease management. The method is trained to detect YR symptoms using reflectance spectrum (VIS–NIR) and a classification algorithm at different stages of YR development to distinguish them from typical defense responses occurring in resistant wheat. The classification method was trained and tested on four different spectral datasets. The results showed that using a full spectral range, a selection of the top 5% significant spectral features, or five typical multispectral bands for early detection of YR in infected plants yielded a true positive rate of ~86%, for infected plants. The same data analysis with digital camera bands provided a true positive rate of 77%. These findings lay the groundwork for the development of high-throughput YR screening in the field implementing multispectral digital camera sensors that can be mounted on autonomous vehicles or a drone as part of an integrated disease management scheme.

Keywords Wheat yellow rust · Random forest · Early detection · Hyper-spectral · Multi-spectral · Spectroscopy · Sensing · Detection

Introduction

Wheat is a major source of starch and energy, and provides substantial amounts of essential or beneficial components such as proteins, vitamins, and phytochemicals (Shewry and Hey 2015). It provides over 20% of the total dietary calories and proteins worldwide for more

✉ Ran Aharoni
tenzoran@gmail.com

Extended author information available on the last page of the article

than 4.5 billion people in more than 100 countries (Goutam et al. 2015; Shiferaw et al. 2013). Meeting the economic challenges resulting from worldwide population growth, increases in energy consumption, the aging population, and the decline in rural areas requires structural changes in agricultural investments and yield economies (FAO 2017). Unfortunately, wheat production is threatened by yellow rust (YR), named also stripe rust, a disease caused by the fungus *Puccinia striiformis* f. sp. *tritici* (*Pst*) which is one of the most devastating fungal diseases globally (Devadas et al. 2009). It is estimated that more than five million tons of wheat production, valued at roughly one billion USD, are lost annually to YR (Beddow et al. 2015). No less critically, global warming is expected to enable certain plant pests and pathogens to spread into larger areas as they evolve into new, more aggressive and adapted strains (Bebber et al. 2013) that are likely to affect crop varieties that are currently resistant or tolerant. One example is the evolution of strains of wheat YR that have adapted to higher temperatures and damaged wheat crops in areas where YR had not been previously reported (FAO 2017). The current approaches for reducing the negative impact of YR on wheat include a combination of breeding for resistance in modern cultivars (Fu et al. 2009; Huang et al. 2016; Uzogara 2000) and precision agriculture technologies that enable disease forecasting and detection (Hodson 2011; Mahlein 2016).

Planting disease-resistant varieties is one of the most efficient wheat YR management strategies. However, due to the co-evolution of the host wheat and the fungal pathogen, *Pst* can overcome the mechanism endowed by YR-resistant genes (Hovmøller et al. 2016; Wellings 2011). However, detecting cases where wheat resistance is overcome by the pathogen can be challenging. For example, resistant wheat varieties may not look green and healthy upon *Pst* inoculation, and will instead have symptom-like yellowing of the leaves due to their Hypersensitive Response (HR) resistance mechanism (Pretorius et al. 2017). This makes HR hard to distinguish in some cases from yellow fungal sporulation on susceptible plants. The recently cloned *Yr15* gene provides resistance to more than 3000 *Pst* isolates with a high level of immunity and only limited HR (Klymiuk et al. 2018), and is a good model for YR spectral studies which can eliminate possible misclassification errors of HR as YR. Nevertheless, the inability to predict the emergence of new strains with high epidemic potential (Ali et al. 2017) means that additional monitoring for pathogens is critical.

Precision agriculture (PA) is generally defined as farming management strategy that involves observing and responding to spatial and temporal variability in the fields, using information delivered by different technologies (Fountas et al. 2015; McBratney et al. 2005). A variety of spectral, visual, thermal, and inertial sensor approaches have been proposed, on spatial and temporal scales ranging from contact probes and ground-based (point detectors, standoff) detectors to (high and low altitude) airborne and satellite detection as reviewed below.

Huang et al. suggested applying a binary linear regression model to multi-temporal airborne hyperspectral (HS) images to identify and map the severity levels of stripe rust infections (Huang et al. 2012). Since HS and high-resolution satellite/airborne observations are relatively rare, Zhang et al. (2011) evaluated a spectral knowledge-based approach using simulated data and moderate resolution satellite HS data. Their estimate of YR severity (disease index, degrees of disease severity) only provided a satisfactory level of accuracy for their simulated data. Another study used remote and standoff sensing to quantify YR levels in winter wheat, and found that a photochemical reflectance index could serve as an indicator for remote HS detection (Huang et al. 2007). Zheng et al. (2019) employed a HS spectrometer to obtain proximity measurements at 1.3 m that could be used for wheat disease detection and prevention in the early-mid growth stage, and estimates of yield losses

in the mid-late growth stage. YR severity was based on a photochemical\anthocyanin reflectance index, calculated for several possible three-band combinations.

Another approach for the close proximity range is to use wireless sensor network (WSN) based applications. WSNs usually employ simple sensors that measure humidity, pressure, and temperature through localization, tracking, micro-radars, and imagery, thereby monitoring a wide range of surroundings to obtain precise information from the field (Díaz et al. 2011; Jawad et al. 2017; Ojha et al. 2015). Since WSNs monitor the surrounding climate and soil they can function as preventive (and preservative) monitoring systems for meteorological wheat disasters (Du et al. 2017), or for predicting disease probability resulting from weather fluctuations (Datir and Wagh 2014). WSNs are useful for expected scenarios involving predetermined program management and enable farmers to determine the actual requirements of crops. Similarly, field-based platforms can combine heterogeneous sensors to collect local information at high spatial and temporal resolutions. Visual, thermal, spectral, and inertial sensors can be harnessed to generate highly informative soil maps based on the ground characteristics at a smaller scale than in traditional remote sensing methods (Milella et al. 2019).

However, both these approaches have shortcomings. Field based and WSN applications need to be positioned and installed in advance, whereas satellite observations have limited temporal and geographical coverage, and suffer from poor resolution, restricted temporal coverage, and environmental (e.g., atmospheric, cloud cover) interference. Fortunately, similar operations can be conducted by Unmanned Aerial Vehicles (UAVs) or drones that enable precision agricultural and smart farming applications from mapping and surveying to crop-dusting and spraying (Tsouros et al. 2019). Unlike satellites, which are expensive and restricted by availability logistics, UAVs are affordable, have cm-scale resolution (Houborg et al. 2015) and are not limited in time or space, which makes them excellent candidates for identifying within-field variations. Another advantage of short range optical measurements compared to remote sensing is that there is much less atmospheric interference.

The studies described above illustrate the potential of spectral reflectance spectroscopy measurements to quantify the severity of plant diseases, and the advantages of a multi-sensor approach to environmental monitoring for prevention and crop management. The current study extends this trend by using optical spectroscopy coupled with data processing that can provide timely detection of YR for PA and farming management. While many conventional treatments for YR are ineffective once the disease is fully developed, some fungicides are considered to have stronger curative activity and can be applied after the disease is first detected (Basandrai et al. 2013); therefore, timely detection of the spatial distribution provides a time window for focused treatment at the individual farm level. In addition, early detection of YR can contribute to decision-making for preventative fungicide applications in non-affected areas within a field. This in turn means that fewer chemicals can be applied without compromising treatment efficacy. One of the key issues in the success of this approach is the tradeoff between system complexity (dimensionality reduction and low cost hardware) and performance. This involves determining the most crucial spectral features for YR detection and the most parsimonious way to classify these features as a function of the severity of disease spread. To respond to this need, the current study addressed the effects of decreasing the dimensionality of the acquired data and the hardware requirements. This was done by applying a statistical learning approach to data interpretation at several data dimensionalities. The preliminary results show that utilizing spectral data in several dimensions is suitable at field scales acquired by UAV or manually, by implementing high level digital camera sensors (available in most smart phones). This approach is

perfectly adapted to the near future of IOT when every farmer will be able to load data to the cloud and use ML central computing algorithms for early disease detection.

Overview of wheat disease detection methods

Many studies have used spectral reflectance measurements to quantify the severity of YR at multiple scales using laboratory, field-based, and satellite technologies. Imaging spectroscopy has been widely implemented to provide reflectance data across a continuous spectrum (i.e., visible and near infrared), and has been successful in previous YR detection approaches. Decreased chlorophyll content and photosynthetic capacity in wheat leaves are signs of general plant stress, such as YR infection (Chang et al. 2013), was shown to be correlated to YR (He et al. 2018). Kuckenberg et al. (2009) suggested that fluorescence imaging could be employed for early pathogen detection and visualization during the early development of YR 2 to 3 days before the manifestation of visual symptoms. However, this requires a pre-darkening adaptation of the leaf that restricts field detection to nighttime. Combined monitoring of chlorophyll and HS imaging can serve to identify YR spores on the 6th day post-inoculation under laboratory conditions (Yao et al. 2019). Zhang et al. (2019) combined high resolution spectral and spatial information through HS imagery at low altitude (30 m) for automated detection of yellow rust with deep convolutional neural networks and RF. They reported 85% accuracy, but used only 3 classes (rust, healthy or others) and some of the data were sampled about 4 weeks from infection, when the disease was already in the severe stages. Handheld spectrometers, along with machine learning algorithms have been employed for the identification and disease index inversion of wheat rust at the canopy level (Qin et al. 2015). The use of UAVs combined with hyperspectral imagers have expanded the capabilities of imaging spectroscopy across larger spatial scales. Multi-temporal airborne hyperspectral images and a binary linear regression model successfully identified and mapped the severity levels of stripe rust infections (Huang et al. 2012). While HS imaging generates valuable detailed spectral and spatial data, HS methods require expensive hardware, suffer from high data dimensionality and low spatial and temporal resolution, require large data storage capacities, and often need more complex analyses, which makes them less appropriate for rapid disease detection (Franke and Menz 2007; Mahlein 2016).

To cut down on these high hardware and data analysis requirements, vegetation indices have been widely developed to detect and classify wheat rust by selecting disease-sensitive bands. Franke and Menz (2007) investigated whether NDVI data processing of multispectral data could serve for early detection of powdery mildew and leaf rust, and concluded that multispectral remote sensing data had low spectral and temporal sensitivity to detecting initial infection stages. Measurements from shorter ranges provided better results, since the amount of mixing between the signal arising from the wheat and the background can be overcome by improved spatial resolution, and also minimizes other artifacts from the atmosphere. For example, a genetic mapping study implemented by a handheld NDVI spectral sensor where the data were subjected to non-linear regression analysis to determine YR disease severity (Pretorius et al. 2017). Proximity spectrometer measurements were collected to calculate three-band spectral indices for wheat disease detection at different wheat growth stages. The authors reported accuracies of 80.6% and 91.9% for the early and late growth stages, respectively (Zheng et al. 2019). The Red Edge Disease Stress Index was developed using Sentinel-2 multispectral imagery and a random forest classifier.

It achieved an overall YR detection accuracy of 84.1% (Zheng et al. 2018). Spectral vegetation indices (SVIs) have been widely used to reduce data dimensionality and detect different plant diseases. Two SVIs were developed from hyperspectral data using an exhaustive search of all wavelengths. This yielded overall YR classification accuracies of 89.5% and 86.5%, but early symptoms of YR were much more difficult to detect (Ashourloo et al. 2014a). Their comparison of several SVIs revealed the sensitivity of SVI values to disease severity, since the collected spectrum became more complex as disease symptoms increased; the classification accuracy was inversely related to disease severity (Ashourloo et al. 2014b).

It is worth noting that the spectral index approach is dependent on the available bands of the sensor and the detection algorithm used. For instance, some studies have suggested that the ratio of reflectance in the green to red region is the most efficient indicator of wheat rust detection (Devadas et al. 2015), whereas others have recommended using the 705 nm and 725 nm bands (Moshou et al. 2004). To further reduce hardware and software requirements, Baresel et al. (2017) suggested using an off the shelf camera as a successful alternative to both spectral and SPAD chlorophyll measurements using basic image analysis procedures such as segmentation and color analysis. Several applications of image analysis in the visible spectrum have been developed to assess disease severity, and diagnose plant diseases and other disorders (Bock et al. 2010). Mahlein (2016) presented sensor imaging and data analysis results for the diagnosis and detection of diseases in crop production based on RGB (Red–Green–Blue channels) sensors but also multi and HS. Automated crop disease pattern recognition systems to identify crop diseases (such as YR) employing severity based segmentation, feature analysis and classification have also been explored (Han et al. 2016; Xu et al. 2017).

The VIS–NIR (800–2500 nm) range provides rapid nondestructive measurements for agriculture, ecology, geology, the food industry and others that can be processed by various analytical techniques (Manley 2014; Sendin et al. 2018). Classification trees; i.e., binary tree structured classifiers, which are a fundamental building block of random forest (RF) classification (Breiman 1996), are useful in predicting the class association of an observation using a large set of covariates (Breiman et al. 1984). Classification, or predicting a class response, is a statistical process that can be realized through statistical modeling approaches such as machine learning (ML). While each algorithm has some advantages, there is no obvious solitary solution to a specific problem. Random Forest provides a measure of predictor importance (Archer and Kimes 2008), and can be used as an effective predictor importance measure in addition to classification by determining the spectral wavelengths that need to be measured. A comparison of RF, probabilistic neural network (PNN), back-propagation neural networks (BPNN), and SVM for the early detection of diseases in grapes in an uncontrolled environment showed that RF outperformed the other methods in terms of classification accuracy (Sandika et al. 2017). Knauer et al. (2017) reported improved classification accuracy when using inherent RF attributes (predetermined ensemble size, picking the required predictors), as well as increased efficiency (by parallel computation) of powdery mildew infection levels in wine grapes. Multispectral, high-resolution satellite data have been used to map the presence of rust in wheat fields in China, using both support vector machines (SVM) and RF classifiers to achieve accuracies of 91.45% and 94.8%, respectively; however, this approach only used binary classifiers and did not distinguish between levels of disease severity (Chen et al. 2018). Another RF-based method was applied to multispectral data collected from a UAV to classify imagery into healthy, moderately diseased, and severely diseased plant material with 89% accuracy 45 days after inoculation (Su et al. 2018). Beyond the performance superiority of

RF, the present study used RF to furnish predictor (i.e. spectral predictor, measured wave-length) selection by harnessing its discriminative ability to provide insights into the most important covariates with respect to the classifier. The RF technique described below is an ensemble classifier; i.e., a predictive model based on individual or multiple classifiers with weighted combinations. This approach can overcome shortcomings such as over-fitting or train-set noise, by combining the results of individual supervised classifiers or a number of different classifiers. RF, as a specific case of bootstrap aggregation (i.e. bagging) can avoid finite size effects of the data, and has been proven to be an accurate supervised learning classification method (Breiman 2001a, b; Svetnik et al. 2003). Bagging makes it possible to use weak and unstable learners such as classification trees, to produce a predictive model by averaging or other voting procedures. As detailed below, the overall aim of this study was to investigate the impact on accuracy of decreasing the dimensionality of acquired spectral data through the applications of a statistical learning approach for data interpretation at several data dimensionalities.

Materials and methods






Biological sample preparation and labeling

The samples were composed of two near isogenic lines (NILs) of bread wheat (*Triticum aestivum*), one with the stripe rust resistance gene *Yr15* (Avocet+*Yr15*) that confers resistance to YR, and one without (Avocet S), which is therefore susceptible to YR. Avocet+*Yr15* carries a 1BS chromosome segment introgressed from wild emmer wheat (*T. turgidum* ssp. *dicoccoides*) that harbors *Yr15* (Klymiuk et al. 2018). To obtain infected leaves, the plants were inoculated at the two-leaf stage with fresh urediniospores of YR isolate #5006 (race 38E134) suspended in Soltrol® 170 light oil (Chevron Phillips Chemical Company, The Woodlands, TX, USA) and dispersed using an airbrush spray gun (Revell, Bunde, Germany). Inoculated plants were kept in a dew chamber (100% humidity) at 10 °C for 16 h in the dark followed by 8 h of light. The plants were then transferred to a growth chamber (70% humidity) at 15 °C with a light intensity of 150 $\mu\text{mol m}^{-2} \text{s}^{-1}$ for 16 h followed by 8 h at 10 °C in darkness for the remainder of the experiment.

A total of 955 samples of susceptible and resistant plants at different stages of YR infection were measured. Representative samples are depicted in Fig. 1, showing healthy wheat leaves and leaves at different stages of the YR and HR development. The figure presents all of the main categories of measured leaves, (from top to bottom): healthy, early HR, developed HR, onset of sporulation and sporulation. The fully developed YR symptoms appear in the bottom leaf (E), which was sampled 14 days post inoculation. In contrast, the healthy (non-infected) leaf (A), is distinguishable by its fresh green appearance. The other leaves are rather similar (B–D), making the application of a unique label challenging for non-pathologists. Thus, two different labelling systems were analyzed here: the biological condition of the leaf, and visual inspection. The 4 *biological labels* were: Susceptible Non-Infected (SNI), Resistant Non-Infected (RNI), Susceptible Infected (SI), Resistant Infected (RI). The 6 *visual labels* were: (1) Green *looking* healthy leaf, (2) HR, early stages, (3) HR, fully developed, (4) Onset of sporulation, (5) Sporulation early stages, and (6) Sporulation final stages.

Note that the visual label system was diagnostic and ignored the biological identity of the sample. It merged leaf stages that would have been identified differently by a

Fig. 1 Representative wheat leaf samples, and labels (for both labeling systems). The examples range from a green fresh healthy leaf to different stages of YR and HR. From top to bottom: **a** healthy (SNI) or resistant non infected (RNI), **b** early stages of HR (resistant infected (RI)), **c** HR fully developed (RI), **d** infected leaf (SI), **e** infected leaf, sporulation (SI)

	Vis-Label	Bio-Label
	1	RNI/SNI
	2	RI
	3	RI
	4	SI
	5	SI

pathologist. The leaf in panel ‘E’; i.e. stage, ‘5’ represents the worst case (within this label) corresponding to day 14 post inoculation (however most leaves with this label were from day 12). Stage 6 (not included in the figure) defined leaves at day 30 post inoculation, and was used as a control to avoid classifying these leaves as an earlier stage. Clearly the differences between the two labeling systems are pronounced. For example, a sample labeled ‘1’ could be applied to any of the biological categories, as long as it did not exhibit any apparent symptoms. Visual labels ‘4’–‘6’ could be assigned to leaves at different stages of the biological SI label. This is depicted in Fig. 1, where each leaf is assigned its appropriate label and all visual labels can apply to panel ‘A’. The two labeling systems; i.e., the ‘theoretical label’ and ‘visual label’ are compared in the Results section.

Each leaf was measured manually at several random sites on its surface. The samples were not preprocessed with extraction techniques or by physically modifying the sample to fit the optical setup, resulting in a certain amount of noise.

Spectral measurements

Spectral measurements in the VIS–NIR wavelengths were conducted with a spectrometer (ASD FieldSpec® 4 Hi-Res) at 350–2500 nm, producing 2151 data points for each measurement. The spectral resolution was 3 nm @ 700 nm/8 nm @ 1400/2100 nm, at a spectral sampling (bandwidth) of 1.4 nm @ 350–1000 nm/1.1 nm @ 1001–2500 nm. The leaves were sampled indoors, fresh from the pot, using a custom accessory sampling contact probe consisting of a Halogen lamp and a collecting fiber as input. In addition to the spectral measurements, leaves at different stages of disease development were photographed using a digital camera (Nikon D810) with a 105 mm macro lens.

Classification

The YR development stages were estimated by assigning the wheat leaves to different classes of disease severity from healthy, through the early stages, to advanced sporulation

(see Fig. 1) before implementing RF. Most models, whether they are a ML (such as NN, KNN, SVM) or discriminant analysis tools, are very useful for classification tasks, but do not provide straightforward insights into the estimator's importance and may demand data dimensionality reduction **prior** to inferring the classifier. RF is a robust classifier that enables these insights, and can able deal with high dimensional data, complex interactions and correlations between variables, which enables estimator selection for data reduction (Hapfelmeier et al. 2014; Kursa 2014).

RF procedure

Before the bagging procedure, the data were divided randomly into a train set (70% of the data), and a test set (30% of the data). Since the classification process is affected by the selection of the training set (Grabmeier and Lambe 2007; Rokach and Maimon 2005), the validation process was carried out in an iterative fashion, where in each iteration a new training set from the entire dataset was randomly chosen, to mitigate possible training set selection effects. The remaining samples, at each iteration, were used for validation. The bagging procedure used a random subset of the training set for training the classifier (each of these subsets contained about two-thirds of the train set) and the remaining third were used as a cross-validation for error estimation (termed “out-of-bag error” OOBerr), where the final classification is obtained by averaging or majority votes of each tree's decision from all sub-sets (Breiman 2001a, b).

First, the OOBerr, or the misclassification probability, was computed to estimate the number of trees required in the RF. Obviously, increasing the number of trees decreases the OOBerr until it stabilizes at a minimal value. Moreover, since in each tree node the predictors are selected randomly, the correlation between the trees in the forest decreases, as does the total error rate. Based on the OOBerr, the importance of the OOB was computed as the difference of a tree's OOBerr before and after random permutation of a predictor variable: if the predictor and the response are not associated, permutation will not influence the error, and the error difference is low (low importance), whereas if the predictor and the response are associated, the error difference will increase as a result of permutation (high importance). The relative OOB importance was used to calculate each predictor's contribution to the learning process. A high importance score indicates that this predictor contributes highly to the learning process. Negative values indicate that this predictor is noisy. Hence, a predictor can impede the learning process.

Predictor selection

The RF classification procedure was applied in four spectral domains: (1) the full spectrum containing 2151 predictors (wavelengths), (2) a reduced predictor space (108 wavelengths) derived by predictor importance, (3) five spectral bands, and (4) three spectral bands, RGB, which are available in off the shelf digital cameras. This fundamental ability of RF to rank the importance of predictors by classifying them as a function of their weight can improve the classification process (Archer and Kimes 2008). Another benefit of RF predictor selection is that it enables dimensionality reduction by selecting the most important features. To simulate these multispectral measurements, a RF classification was applied to five spectral bands, resampled according to Altum™ by MicaSense (<https://www.micasense.com>), as detailed in Table 1.

Table 1 Spectral bands for the five multispectral bands, Altum™ by MicaSense

Band	Center (nm)	Band-width (nm)
Blue	475	20
Green	560	20
Red	668	10
Red edge	717	10
Near infra-red	840	40

Next standard consumer digital cameras were examined. RGB camera channels were simulated by using the corresponding RGB bands. Table 2 details the RGB spectral bands in typical RGB cameras.

The database, composed of 955 spectral measurements, was analyzed using both labeling systems, in all four domains. The results are presented as a confusion matrix comparing the true class (y-axis) to the class predicted by the classifier (x-axis), as shown in Figs. 4, 6, and 7. The diagonal terms represent successful classification and the off-diagonal represents incorrect classification. All quantitative terms are also represented by color. The correctly classified measurements, (termed ‘accuracy’), are defined as the ratio of the true terms (diagonal terms) to the total number of true and false terms (the whole matrix). Each chart is accompanied by a row-normalized summary and a column-normalized summary. The vertical row-normalized summary represents the true positive and false positive rates (which represents the class-wise recalls; i.e., the percentages of correctly/incorrectly classified observations for each true class). The horizontal column-normalized summary represents the positive predictive values (which represents the class-wise precisions; i.e., the percentages of correctly and incorrectly classified observations for each predicted class).

Results

Data exploration

Typical infected and non-infected wheat leaves are shown in Fig. 2a, where the leaves on the right are green and healthy, and the leaves on the left manifest fully developed symptoms with abundant sporulation on the susceptible Avocet S plants (label ‘6’). Figure 2b presents a typical spectrum from fully developed YR, obtained by dividing the trace from a leaf with a fully developed YR by the trace of a healthy leaf. This ideal clean spectrum of YR spores does not reflect the expected spectrum of infected leaves at any stage; however, it presents the main absorption peaks of YR. These peaks are

Table 2 Typical spectral bands for RGB commercial digital cameras

Band	Center (nm)	Bandwidth (nm)
Blue	440	120
Green	525	150
Red	630	140

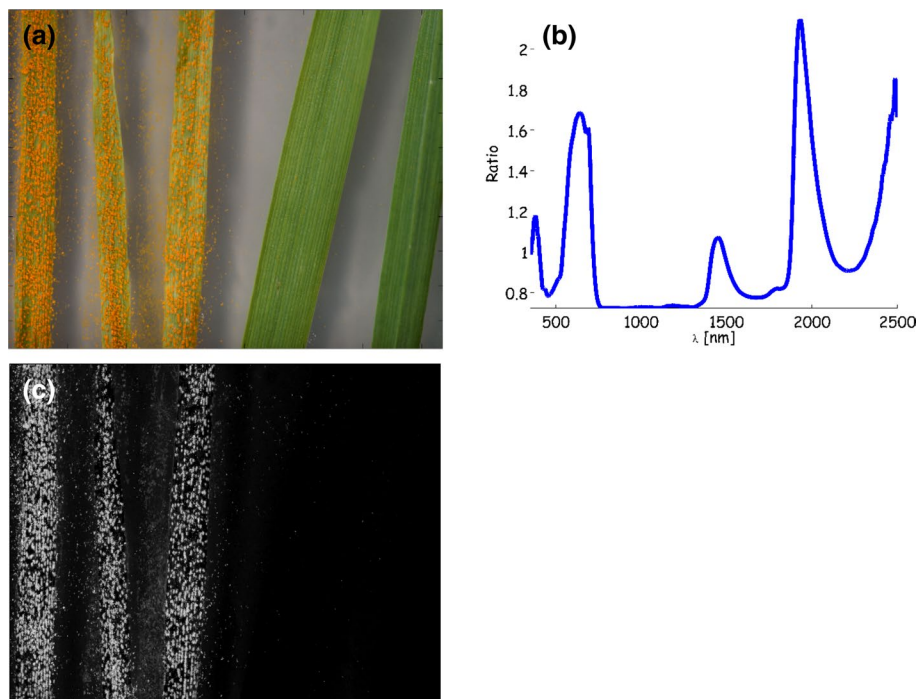


Fig. 2 Visual appearance and spectral response of infected and healthy leaves. **a** Leaves with developed YR infection in the final stages (left), compared to healthy leaves (right). **b** VIS–NIR spectrum of the infected leaves of figure (a). **c** Enhancement of figure (a) by subtracting the green from the red channel

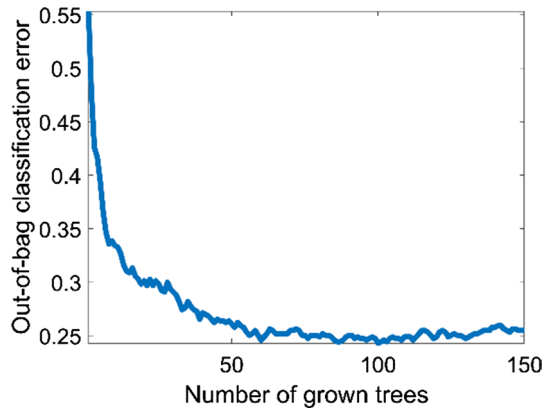
located around 668 nm, 1450 nm, and 1935 nm. Two additional peaks, often truncated, are located at the edges of the spectrum at 380 nm and 2470 nm. As indicated in Fig. 2b (and Fig. 5b) a considerable number of significant predictors were found in the visual and near IR spectrum (VIS–NIR). Figure 2c presents the data from the RGB photo of Fig. 2a after processing, in which the data in the green channel were subtracted from the red channel. It shows that even with a minimal dataset of a few channels, fully developed YR can be detected.

The results above suggest that fully developed YR can be detected using relatively simple means. The next sections describe how a RF classification of wheat plants can enable timely detection of infected crops for the cases shown in Fig. 1, in which the difference between leaves at different stages are difficult to differentiate.

One of the key parameters when using a RF classifier is the size of the forest; namely, how many decision trees are included in the classification process. Figure 3 shows the OOBerr (Breiman 2001a, b) as a function of the number of trees, for the dataset described above and utilizing the entire spectrum of each measurement. The graph shows that the error decreases with the number of trees up to about 100 trees, where it reaches its minimum value of 25%. The following RF calculation used 150 trees to verify that the OOBerr was at its minimal value.

In order to account for possible variations in the results due to the random selection of training set and out-of-bag samples, the classification was repeated 10 000 times. The resulting standard deviation was < 1% which is negligible in this case.

Fig. 3 An example of the Out-Of-Bag error rate vs. number of grown trees used for classification. The error rate decreases to a constant value of ~25–28% when the number of trees exceeds 60



Classification of hyper-spectral data

The RF classification was applied to the dataset. Figure 4 shows the classification into biological labels (a) (i.e. SNI, RNI, SI, RI) and visual labels (b). The classification accuracy was 81.5% and 74.2% for the biological and visual classifications, respectively. For the biological labels, the true positive rates (TPR) for the infected SI and RI labels were 86.5% and 83.8%, respectively. For the visual labels, the TPR was 87.5% for final stages of sporulation (label 6). The TPR for labels 4 (onset of sporulation) and 5 (sporulation early stages) were 53.3%, and 92.2%, respectively. Note that the green healthy areas of the leaf spatially dominated the sampled area in all measurements. This is indicated by the higher misclassification of label 2 (HR, early stages) as 1 (green *looking* healthy leaf). This was expected because the spectral (and visual) differences between samples labeled as 1 or 2 were minor.

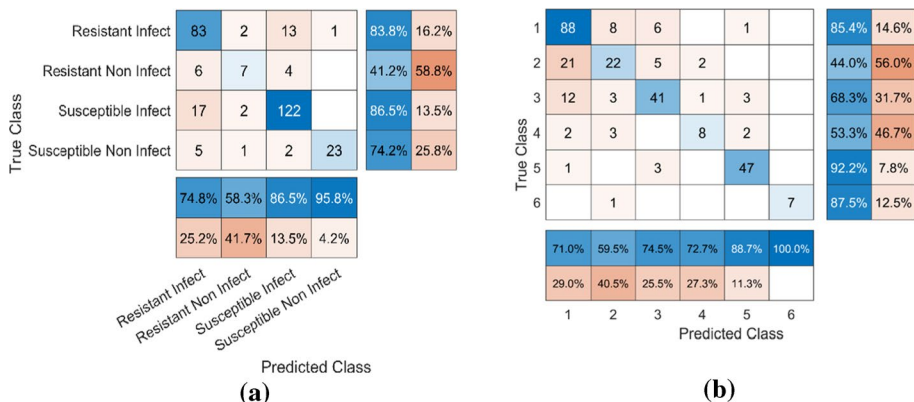


Fig. 4 Confusion matrix for the RF classification with the full spectrum. The numbers located on the diagonal of the matrices indicate the number of accurate classifications for each class; the off-axis are the false identifications. **a** Using the biological set of labels. **b** Using the visual set of labels

Fig. 5 Predictor importance (OOB importance), indicating the contribution of each predictor to the RF. The top 5% are marked in black

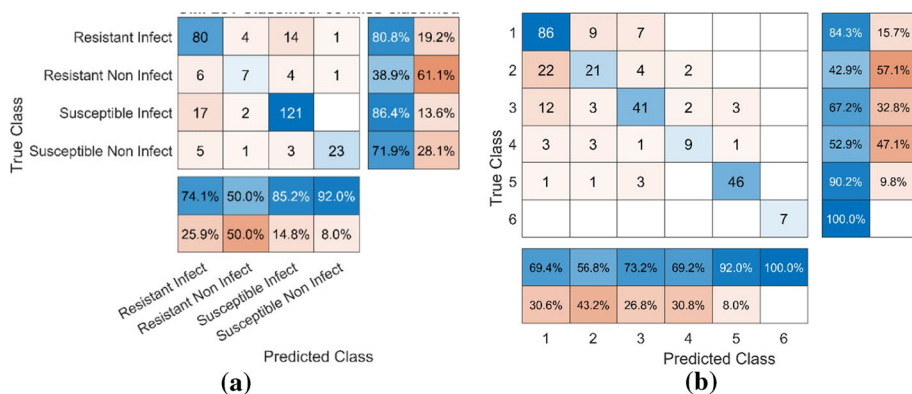
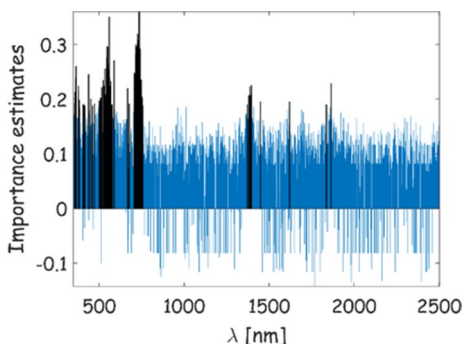


Fig. 6 Confusion matrices showing the classification using the selected predictors (top 5%): **a** biological labels; **b** visual labels. The classification accuracy was comparable to the one obtained using the entire spectrum

Classification using reduced predictor space

The properties of all predictors were examined prior to reduction, by calculating the per sample error rate; namely, the relative misclassification for each sample. This error rate was obtained as follows: 400 train sets were selected randomly, and each train set was processed 100 times using RF, which yielded 40 000 forests. Due to the noisy nature of the measurements, some of the samples were more prone to misclassification than others. However, there were no chronically defective samples that could not be classified correctly; i.e., no outliers. The error rate ranged from negligible to as much as 6.9%, with a mean of 0.2%, a standard deviation of 0.22, and a median of 0.1%. Figure 5 depicts the predictor importance for all 2151 spectral channels. It is noteworthy that there are numerous negative values, indicating insignificant spectral channels across the spectrum. The top 5% significant channels are located around 500–700 nm, 1400 nm, and 1900 nm, which is consistent with the reflectance spectrum presented in Fig. 2b.

Based on Fig. 5, the data were classified with an identical RF procedure using the selected predictor space (Fig. 6). The results were very similar to those obtained using the full spectrum, with a slight decrease of about 1.5% from 81.5 to 79.9% (biological

labels), and from 74.2 to 73.1% (visual labels). The performance for the significant labels; i.e., RI and SI (biological labels), and 5 (visual labels) were also similar.

The RF classification results using five bands (centered at 475, 560, 668, 717, and 840 nm; see Table 1) are shown in the confusion matrix in Fig. 7a, b. It shows that minimizing the spectral data for these five bands degraded classifier performance slightly, yielding an accuracy of 78.5% and 65.1% for the biological and visual label classifications, respectively. The TPR for SI and label ‘5’ were 85.8% and 88%, respectively.

Further reduction of the feature space to three wave lengths (‘R’, ‘G’, and ‘B’ see Table 2), reduced the overall classifier performance, as shown in Fig. 7c, d. The accuracy for the biological and visual labels was 54.8% for the former and 65.8% for the latter. However, the TPR for the infected plants remained high at 77.7% for SI and 78.4% for visual label ‘5’, making this easy setup suitable for simple tasks such as the detection of fully sporulated YR.

Comparison: levels of predictor spaces and labeling systems

Figure 8 summarizes the results for the total classification accuracy (dashed line) and the specific accuracy; i.e., TPR (solid line), for both the biological labeling system (red) and

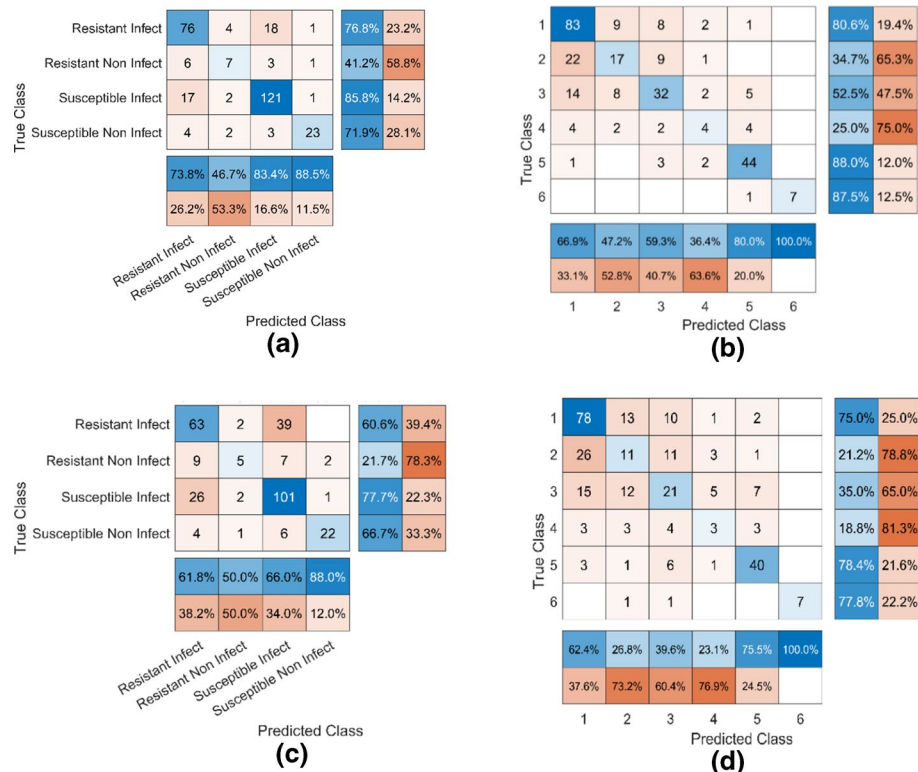
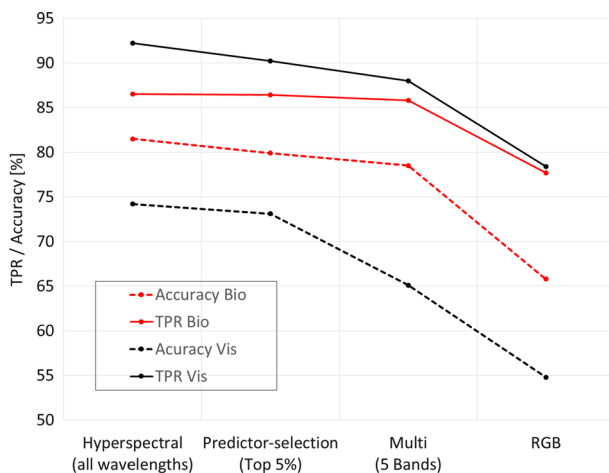


Fig. 7 Classification using 5 and 3 spectral bands for both labeling systems. **a** and **b** confusion matrices obtained using 5 spectral bands that are available in a commercial agricultural drone sensor (**a** biological labels, **b** visual labels). Similarly **c** and **d** present the confusion matrices using three spectral bands available in digital cameras (**c** biological labels, **d** visual labels)

Fig. 8 Accuracy, and true positive rates (TPR), obtained using four levels of the predictors set: hyperspectral (all 2151 wavelengths), predictor-selection (top 5% important); multi-spectral (5-bands), and RGB. The accuracy is defined as the total accuracy of the classification, and TPR is the true positive rate for visual label ‘5’ and biological label SI



the visual labeling system (black). The TPR depicts the key SI and ‘5’ (early stages of sporulation) labels. It shows that in all cases the overall accuracy; i.e., the correct classification of the disease stages was lower than the TPR. An accuracy of 77.7% was obtained with a multispectral camera. At further simplification of the sensor with an RGB sensor, the level of accuracy is unacceptable, but the TPR was higher than 80% and may be useful in some scenarios. It also shows that while the biological labeling system exhibits better performance for accuracy, the visual labeling approach outperforms for the TPR.

For timely detection of YR, accuracy is less informative, and the ‘specific accuracy’, or TPR, of the relevant SI and label ‘5’ leaves should be taken into account. In this case, applying the biological labeling means that all stages of the disease are subsumed under a single label. This pools leaves at different stages of YR from fully developed symptoms to leaves with no apparent spectral signature of YR. This results in a lower TPR for the biological labeling system, as a result of possible misclassifications of green leaves in the early non-symptomatic stages. Likewise, in the confusion matrices for visual labeling, the TPR improves as YR and HR symptoms are more severe. This is probably due to the presence of green areas in all the samples, which decreases as YR/HR symptoms appear.

Discussion and conclusion

Timely YR detection is crucial for economic decisions about disease management, in particular fungicide applications. While many fungicides are sprayed as a preventative measure, some products can reduce the severity of symptoms after the disease has manifested (De Wolf 2010). For example, the triazole class of fungicides is generally considered to have stronger curative activity and can be applied after the disease is detected in the field (Basandrai et al. 2013). Therefore, if YR is observed early enough, and the appropriate treatment is applied at the right time, further sporulation and spreading of YR within the field and to neighboring fields can be reduced or completely prevented, thus reducing disease severity and preserving yield. The detection of YR at early stages can also help enable site-specific disease management based on disease symptoms, rather than relying on unnecessary fungicide applications. This can reduce costs and the environmental impact

associated with their application (Jørgensen et al. 2014). Timely detection combined with a simple accessible means can contribute to eradicating escalating YR epidemics (www.wheatrust.org), and responds to warnings issued by the food and agriculture organization of the United Nations concerning the rapid unexpected spread of rust diseases in wheat. As mentioned above, using resistant varieties is a common ecological way to defeat crop diseases. However, the *Pst* pathogen can mutate and become virulent on currently resistant wheat varieties. Thus, the ability to distinguish YR from HR is important. As seen in Figs. 4, 6, and 7, the misclassifications of YR early stages (label 5) and HR stages (labels 2, 3) are negligible. In all the confusion matrices, the values of the intersection of row 5 and columns [2, 3] are low. This suggests that YR can be detected in fields where resistant wheat varieties expressing HR in response to *Pst* inoculation are planted.

The visual labeling system makes it possible to describe the critical stages of disease development, instead of using a single label, and outperforms biological labeling, as seen in Fig. 8. It is likely to be enhanced when labeling the leaves with majority voting by multiple individuals, due to the inconsistent nature of human labeling. More disease stages (labels) could also be considered. Clearly, the RF predictor selection based on importance only had a slight effect on performance. The RF predictor space reduction was based on the ability of the RF classifier predictor, to rank in terms of importance, which predicted the significance of these specific wavelengths. The, the multi-spectral sensor was chosen for agricultural needs since the red edge band (712–723 nm) is indicative of various stress symptoms in chlorophyll-containing vegetation (Filella and Peñuelas 1994; Guo et al. 2018). The other bands also contained the spectral features of YR, as seen in Figs. 2b and 5. This explains why the decrease in TPR when using multi-spectral approach was negligible, and justifies its use, as described above. Although commercial digital camera channels were not designed for agricultural considerations, RGB imagers have been suggested for agricultural applications as a complement to other spectral devices in developing SVI for disease severity estimation (Ashourloo et al. 2014a, b), phenotyping (Maimaitijiang et al. 2017), and also as spatial information for YR diagnosis and grape diseases classification with image processing (Sandika et al. 2017; Xu et al. 2017). Franke and Menz (2007) also suggested controlling for the success of fungicide treatments, using the classification of multispectral and multi-temporal remote sensing of wheat diseases. However, their method is only effective at advanced growth stages, because of low spatial and temporal issues. This led them to argue that short-range detection systems and remote sensing data should be considered as complementary strategies for precision agriculture applications. In the current study, the green appearance of healthy leaves, as well as stress in general and YR in particular all have visible effects, most of which are in the ‘G’ and ‘R’ channels of commercial RGB bands. By expanding the data by using spatial information and image processing, the noticeable decrease when using only the RGB presented bands can be significantly overcome.

The method of YR detection presented here was based on the inoculation of wheat seedlings in a highly controlled laboratory environment. However, the reactions of seedlings and adult wheat plants, as well as their expression in laboratory and field conditions may differ. Thus, this method should be evaluated under field conditions for adult wheat plants prior to wider application. At this stage, it is hard to compare the results, which are based on seedling reactions in controlled conditions, to other methods of YR detection in the field. Nevertheless, it has potential advantages for applications in small farms that cannot afford satellite imaging or other expensive and sophisticated equipment. Another point to be considered is that a realistic scenario might involve large sample variations and interference from background materials. Here, in the preliminary

analyses, the spectral response of red loam soil collected in Ness-Ziona (Israel) was also measured and added to the dataset, which resulted in 100% accurate labeling of the soil with negligible to no effect on the classification accuracy of the wheat leaves.

In scenarios when YR appears unexpectedly on varieties known to be resistant in the past, a rapid response and real-time actions are required to prevent the further spread of the disease. Due to the random nature of these situations, simple hardware and machine learning techniques can be used for geographic locations that are not under constant monitoring to detect early stage YR. This study thus constitutes a first step towards developing robust disease detection models that can be deployed in the field for scouting by characterizing and classifying rust in a controlled environment. In terms of the tradeoff between system simplicity and efficiency hyperspectral sensors provided a more accurate classification of YR and may be able to detect other diseases. However, the vast deployment of hyperspectral sensors is likely to be expensive compared to simpler multispectral sensors. Hence, the combination of multispectral sensors and hyperspectral sensors can provide good coverage and performance. Future work will concentrate on the extension of this study to other diseases, the validation of the results in field experiments and the investigation of combinations of several sensors to find the right balance between system complexity and efficiency.

Summary

This work examined the utilization of spectral data at several levels of dimensionality reduction to enable the use of low-cost multispectral or RGB systems, and presented preliminary results. The RF classifier, a robust algorithm, yielded reliable and high detection rates of early stages of YR with a multi-spectral sensor, 12 days post *Pst* infection. Plants expressing HR resistance, which appear similar to some early stages of YR susceptible plants were successfully differentiated from actual YR development in susceptible wheat genotypes. These results lay the foundation for high-throughput YR screening in the field using autonomous vehicles and commercially available multispectral sensors as part of an integrated pathogen management scheme that utilizes both resistant varieties and precision agriculture technologies for YR detection and monitoring.

Selecting the top 5% most important predictors for RF classification had little effect on classifier performance. This can be attributed to the fact that the RF identified the absorption bands of YR based on its contrast with the green background, which is common to all measurements. Reducing the number of predictors further is advantageous for the application of simple robust system. Thus, the performance of an agricultural multi-spectral sensor with only five bands was simulated and showed that accurate detection of YR using this simplified setup is possible. Preliminary results when using a digital camera was also reported, and generated reasonable results that can be used to supplement imaged spatial data in future research.

Further work is required to devise a system capable of sensing in a rapidly changing environment, and determining its optimal analysis procedure. The utilization of autonomous vehicles is likely to develop in the near future given the advantages of short range monitoring by satellite observations. Both autonomous vehicles and manual photography can benefit from information and communication technologies and the IOT revolution, when every farmer will be able to load data to the cloud with affordable hardware.

References

- Ali, S., Rodriguez-Algaba, J., Thach, T., Sørensen, C. K., Hansen, J. G., Lassen, P., et al. (2017). Yellow rust epidemics worldwide were caused by pathogen races from divergent genetic lineages. *Frontiers in Plant Science*, 8, 1057. <https://doi.org/10.3389/fpls.2017.01057>.
- Archer, K. J., & Kimes, R. V. (2008). Empirical characterization of random forest variable importance measures. *Computational Statistics & Data Analysis*, 52(4), 2249–2260. <https://doi.org/10.1016/j.csda.2007.08.015>.
- Ashourloo, D., Mobasheri, M., & Huete, A. (2014a). Developing two spectral disease indices for detection of wheat leaf rust (*Puccinia triticina*). *Remote Sensing*, 6(6), 4723–4740. <https://doi.org/10.3390/rs6064723>.
- Ashourloo, D., Mobasheri, M., & Huete, A. (2014b). Evaluating the effect of different wheat rust disease symptoms on vegetation indices using hyperspectral measurements. *Remote Sensing*, 6(6), 5107–5123. <https://doi.org/10.3390/rs6065107>.
- Baresel, J. P., Rischbeck, P., Hu, Y., Kipp, S., Hu, Y., Barmer, G., et al. (2017). Use of a digital camera as alternative method for non-destructive detection of the leaf chlorophyll content and the nitrogen nutrition status in wheat. *Computers and Electronics in Agriculture*, 140, 25–33. <https://doi.org/10.1016/j.compag.2017.05.032>.
- Basandrai, A. K., Sharma, B., & Basandrai, D. (2013). Efficacy of triazole fungicides for the integrated management of yellow rust, leaf rust and powdery mildew of wheat. *Plant Disease Research*, 28(2), 135–139.
- Bebber, D. P., Ramotowski, M. A. T., & Gurr, S. J. (2013). Crop pests and pathogens move polewards in a warming world. *Nature Climate Change*, 3(11), 985–988. <https://doi.org/10.1038/nclimate1990>.
- Beddow, J. M., Pardey, P. G., Chai, Y., Hurley, T. M., Kriticos, D. J., Braun, H. J., et al. (2015). Research investment implications of shifts in the global geography of wheat stripe rust. *Nature Plants*, 1(Sep-tember), 1–5. <https://doi.org/10.1038/nplants.2015.132>.
- Bock, C. H., Poole, G. H., Parker, P. E., & Gottwald, T. R. (2010). Plant disease severity estimated visually, by digital photography and image analysis, and by hyperspectral imaging. *Critical Reviews in Plant Sciences*, 29(2), 59–107. <https://doi.org/10.1080/07352681003617285>.
- Breiman, L. (1996). Bagging predictors. *Machine Learning*, 24(2), 123–140. <https://doi.org/10.1007/BF00058655>.
- Breiman, L. (2001a). Machine learning. *Statistics Department, University of California, Berkeley*, 45(1), 5–32. <https://doi.org/10.1023/a:1010933404324>.
- Breiman, L. (2001b). Random forests. *Machine Learning*, 45(1), 5–32. <https://doi.org/10.1023/A:1010933404324>.
- Breiman, L., Friedman, J., Stone, C., & Olshen, R. (1984). *Classification and regression trees*. Boca Raton: CRC Press.
- Chang, Q., Liu, J., Wang, Q., Han, L., Liu, J., Li, M., et al. (2013). The effect of *Puccinia striiformis* f. sp. tritici on the levels of water-soluble carbohydrates and the photosynthetic rate in wheat leaves. *Physiological and Molecular Plant Pathology*, 84(1), 131–137. <https://doi.org/10.1016/j.pmp.2013.09.001>.
- Chen, D., Shi, Y., Huang, W., Zhang, J., & Wu, K. (2018). Mapping wheat rust based on high spatial resolution satellite imagery. *Computers and Electronics in Agriculture*, 152, 109–116. <https://doi.org/10.1016/j.compag.2018.07.002>.
- Datir, S., & Wagh, S. (2014). Monitoring and detection of agricultural disease using wireless sensor network. *International Journal of Computer Applications*, 87.
- De Wolf, E. (2010). Wheat stripe rust. *Kansas State University* (EP-167), 1–2. Retrieved April 6, 2020, from www.ksre.ksu.edu.
- Devadas, R., Lamb, D. W., Backhouse, D., & Simpfordorfer, S. (2015). Sequential application of hyperspectral indices for delineation of stripe rust infection and nitrogen deficiency in wheat. *Precision Agriculture*, 16(5), 477–491. <https://doi.org/10.1007/s11119-015-9390-0>.
- Devadas, R., Lamb, D. W., Simpfordorfer, S., & Backhouse, D. (2009). Evaluating ten spectral vegetation indices for identifying rust infection in individual wheat leaves. *Precision Agriculture*, 10(6), 459–470. <https://doi.org/10.1007/s11119-008-9100-2>.
- Díaz, S. E., Pérez, J. C., Mateos, A. C., Marinescu, M. C., & Guerra, B. B. (2011). A novel methodology for the monitoring of the agricultural production process based on wireless sensor networks. *Computers and Electronics in Agriculture*, 76(2), 252–265. <https://doi.org/10.1016/j.compag.2011.02.004>.
- Du, K., Sun, Z., Zheng, F., Chu, J., & Ma, J. (2017). Monitoring system for wheat meteorological disasters using wireless sensor networks. In *2017 ASABE annual international meeting*. American Society of Agricultural and Biological Engineers. <https://doi.org/10.13031/aim.201700055>.
- FAO. (2017). *The future of food and agriculture—Trends and challenges*. Rome: FAO.

- Filella, I., & Peñuelas, J. (1994). The red edge position and shape as indicators of plant chlorophyll content, biomass and hydric status. *International Journal of Remote Sensing*, 15(7), 1459–1470. <https://doi.org/10.1080/01431169408954177>.
- Fountas, S., Aggelopoulou, K., & Gemtos, T. A. (2015). Precision agriculture: Crop management for improved productivity and reduced environmental impact or improved sustainability. In *Supply chain management for sustainable food networks* (pp. 41–65). Chichester, UK: Wiley. <https://doi.org/10.1002/9781118937495.ch2>.
- Franke, J., & Menz, G. (2007). Multi-temporal wheat disease detection by multi-spectral remote sensing. *Precision Agriculture*, 8(3), 161–172. <https://doi.org/10.1007/s11119-007-9036-y>.
- Fu, D., Uauy, C., Distelfeld, A., Blechl, A., Epstein, L., Chen, X., et al. (2009). A kinase-START gene confers temperature-dependent resistance to wheat stripe rust. *Science*, 323(5919), 1357–1360. <https://doi.org/10.1126/science.1166289>.
- Goutam, U., Kukreja, S., Yadav, R., Salaria, N., Thakur, K., & Goyal, A. K. (2015). Recent trends and perspectives of molecular markers against fungal diseases in wheat. *Frontiers in Microbiology*. <https://doi.org/10.3389/fmicb.2015.00861>.
- Grabmeier, J., & Lambe, L. (2007). Decision trees for binary classification variables grow equally with the Gini impurity measure and Pearson's chi-square test. *International Journal of Business*, 2(2), 213–226. <https://doi.org/10.1504/IJBIDM.2007.013938>.
- Guo, B.-B., Zhu, Y.-J., Feng, W., He, L., Wu, Y.-P., Zhou, Y., et al. (2018). Remotely estimating aerial N uptake in winter wheat using red-edge area index from multi-angular hyperspectral data. *Frontiers in Plant Science*, 9, 675. <https://doi.org/10.3389/fpls.2018.00675>.
- Han, L., Haleem, M. S., & Taylor, M. (2016). Automatic detection and severity assessment of crop diseases using image pattern recognition. *Studies in Computational Intelligence*, 647, 283–300. https://doi.org/10.1007/978-3-319-33353-3_15.
- Hapfelmeier, A., Hothorn, T., Ulm, K., & Strobl, C. (2014). A new variable importance measure for random forests with missing data. *Statistics and Computing*, 24(1), 21–34. <https://doi.org/10.1007/s11222-012-9349-1>.
- He, R., Li, H., Qiao, X., & Jiang, J. (2018). Using wavelet analysis of hyperspectral remote-sensing data to estimate canopy chlorophyll content of winter wheat under stripe rust stress. *International Journal of Remote Sensing*, 39(12), 4059–4076. <https://doi.org/10.1080/01431161.2018.1454620>.
- Hodson, D. P. (2011). Shifting boundaries: Challenges for rust monitoring. *Euphytica*, 179(1), 93–104. <https://doi.org/10.1007/s10681-010-0335-4>.
- Houborg, R., Fisher, J. B., & Skidmore, A. K. (2015). Advances in remote sensing of vegetation function and traits. *International Journal of Applied Earth Observation and Geoinformation*. <https://doi.org/10.1016/j.jag.2015.06.001>.
- Hovmøller, M. S., Walter, S., Bayles, R. A., Hubbard, A., Flath, K., Sommerfeldt, N., et al. (2016). Replacement of the European wheat yellow rust population by new races from the centre of diversity in the near-Himalayan region. *Plant Pathology*, 65(3), 402–411. <https://doi.org/10.1111/ppa.12433>. <https://www.micasense.com/>. (n.d.).
- Huang, L., Raats, D., Sela, H., Klymiuk, V., Lidzbarsky, G., Feng, L., et al. (2016). Evolution and adaptation of wild emmer wheat populations to biotic and abiotic stresses. *Annual review of Phytopathology*, 54(1), 279–301. <https://doi.org/10.1146/annurev-phyto-080614-120254>.
- Huang, L. S., Zhao, J. L., Zhang, D. Y., Yuan, L., Dong, Y. Y., & Zhang, J. C. (2012). Identifying and mapping stripe rust in winter wheat using multi-temporal airborne hyperspectral images. *International Journal of Agriculture and Biology*, 14(5), 697–704.
- Huang, W., Lamb, D. W., Niu, Z., Zhang, Y., Liu, L., & Wang, J. (2007). Identification of yellow rust in wheat using in situ spectral reflectance measurements and airborne hyperspectral imaging. *Precision Agriculture*, 8(4–5), 187–197. <https://doi.org/10.1007/s11119-007-9038-9>.
- Jawad, H. M., Nordin, R., Gharghan, S. K., Jawad, A. M., & Ismail, M. (2017). Energy-efficient wireless sensor networks for precision agriculture: A review. *Sensors*. <https://doi.org/10.3390/s17081781>.
- Jørgensen, L. N., Hovmøller, M. S., Hansen, J. G., Lassen, P., Clark, B., Bayles, R., et al. (2014). IPM strategies and their dilemmas including an introduction to www.eurowheat.org. *Journal of Integrative Agriculture*. [https://doi.org/10.1016/s2095-3119\(13\)60646-2](https://doi.org/10.1016/s2095-3119(13)60646-2).
- Klymiuk, V., Yaniv, E., Huang, L., Raats, D., Fatiukha, A., Chen, S., et al. (2018). Cloning of the wheat Yr15 resistance gene sheds light on the plant tandem kinase-pseudokinase family. *Nature Communications*. <https://doi.org/10.1038/s41467-018-06138-9>.
- Knauer, U., Matros, A., Petrovic, T., Zanker, T., Scott, E. S., & Seiffert, U. (2017). Improved classification accuracy of powdery mildew infection levels of wine grapes by spatial-spectral analysis of hyperspectral images. *Plant Methods*, 13(1), 47. <https://doi.org/10.1186/s13007-017-0198-y>.

- Kuckenberg, J., Tartachnyk, I., & Noga, G. (2009). Temporal and spatial changes of chlorophyll fluorescence as a basis for early and precise detection of leaf rust and powdery mildew infections in wheat leaves. *Precision Agriculture*, 10(1), 34–44. <https://doi.org/10.1007/s11119-008-9082-0>.
- Kursa, M. B. (2014). Robustness of random forest-based gene selection methods. *BMC Bioinformatics*. <https://doi.org/10.1186/1471-2105-15-8>.
- Mahlein, A. K. (2016). Plant disease detection by imaging sensors—Parallels and specific demands for precision agriculture and plant phenotyping. *Plant Disease*. <https://doi.org/10.1094/pdis-03-15-0340-fe>.
- Maimaitijiang, M., Ghulam, A., Sidike, P., Hartling, S., Maimaitiyiming, M., Peterson, K., et al. (2017). Unmanned aerial system (UAS)-based phenotyping of soybean using multi-sensor data fusion and extreme learning machine. *ISPRS Journal of Photogrammetry and Remote Sensing*, 134, 43–58. <https://doi.org/10.1016/j.isprsjprs.2017.10.011>.
- Manley, M. (2014). Near-infrared spectroscopy and hyperspectral imaging: Non-destructive analysis of biological materials. *Chemical Society Reviews*, 43(24), 8200–8214. <https://doi.org/10.1039/c4cs00062e>.
- McBratney, A., Whelan, B., Ancev, T., & Bouma, J. (2005). Future directions of precision agriculture. *Precision Agriculture*, 6, 7–23. <https://doi.org/10.1007/s11119-005-0681-8>.
- Milella, A., Reina, G., & Nielsen, M. (2019). A multi-sensor robotic platform for ground mapping and estimation beyond the visible spectrum. *Precision Agriculture*, 20(2), 423–444. <https://doi.org/10.1007/s11119-018-9605-2>.
- Moshou, D., Bravo, C., West, J., Wahlen, S., McCartney, A., & Ramon, H. (2004). Automatic detection of “yellow rust” in wheat using reflectance measurements and neural networks. *Computers and Electronics in Agriculture*. <https://doi.org/10.1016/j.compag.2004.04.003>.
- Ojha, T., Misra, S., & Raghuvanshi, N. S. (2015). Wireless sensor networks for agriculture: The state-of-the-art in practice and future challenges. *Computers and Electronics in Agriculture*. <https://doi.org/10.1016/j.compag.2015.08.011>.
- Pretorius, Z. A., Lan, C. X., Prins, R., Knight, V., McLaren, N. W., Singh, R. P., et al. (2017). Application of remote sensing to identify adult plant resistance loci to stripe rust in two bread wheat mapping populations. *Precision Agriculture*, 18(4), 411–428. <https://doi.org/10.1007/s11119-016-9461-x>.
- Qin, F., Liu, Q., Ruan, L., Wang, R., Ma, Z., Li, X., et al. (2015). Identification and disease index inversion of wheat stripe rust and wheat leaf rust based on hyperspectral data at canopy level. *Journal of Spectroscopy*. <https://doi.org/10.1155/2015/651810>.
- Rokach, L., & Maimon, O. (2005). Top-down induction of decision trees classifiers - A survey. *IEEE Transactions on Systems, Man and Cybernetics Part C: Applications and Reviews*, 35(4), 476–487. <https://doi.org/10.1109/TSMCC.2004.843247>.
- Sandika, B., Avil, S., Sanat, S., & Srinivasu, P. (2017). Random forest based classification of diseases in grapes from images captured in uncontrolled environments. *International Conference on Signal Processing Proceedings, ICSP*. <https://doi.org/10.1109/icsp.2016.7878133>.
- Sendin, K., Williams, P. J., & Manley, M. (2018). Near infrared hyperspectral imaging in quality and safety evaluation of cereals. *Critical Reviews in Food Science and Nutrition*, 58(4), 575–590. <https://doi.org/10.1080/10408398.2016.1205548>.
- Shewry, P. R., & Hey, S. J. (2015). The contribution of wheat to human diet and health. *Food and Energy Security*, 4(3), 178–202. <https://doi.org/10.1002/FES3.64>.
- Shiferaw, B., Smale, M., Braun, H. J., Duveiller, E., Reynolds, M., & Muricho, G. (2013). Crops that feed the world 10. Past successes and future challenges to the role played by wheat in global food security. *Food Security*, 5(3), 291–317. <https://doi.org/10.1007/s12571-013-0263-y>.
- Su, J., Liu, C., Coombes, M., Hu, X., Wang, C., Xu, X., et al. (2018). Wheat yellow rust monitoring by learning from multispectral UAV aerial imagery. *Computers and Electronics in Agriculture*, 155, 157–166. <https://doi.org/10.1016/j.compag.2018.10.017>.
- Svetnik, V., Liaw, A., Tong, C., Christopher Culbertson, J., Sheridan, R. P., & Feuston, B. P. (2003). Random forest: A classification and regression tool for compound classification and QSAR modeling. *Journal of Chemical Information and Computer Sciences*, 43(6), 1947–1958. <https://doi.org/10.1021/ci034160g>.
- Tsouros, D. C., Bibi, S., & Sarigiannidis, P. G. (2019). A review on UAV-based applications for precision agriculture. *Information*. <https://doi.org/10.3390/info10110349>.
- Uzogara, S. G. (2000). The impact of genetic modification of human foods in the 21st century: A review. *Biotechnology Advances*, 18(3), 179–206. [https://doi.org/10.1016/S0734-9750\(00\)00033-1](https://doi.org/10.1016/S0734-9750(00)00033-1).
- Wellings, C. R. (2011). Global status of stripe rust: A review of historical and current threats. *Euphytica*. <https://doi.org/10.1007/s10681-011-0360-y>.
- Xu, P., Wu, G., Guo, Y., Chen, X., Yang, H., & Zhang, R. (2017). Automatic wheat leaf rust detection and grading diagnosis via embedded image processing system. *Procedia Computer Science*, 107, 836–841. <https://doi.org/10.1016/j.procs.2017.03.177>.

- Yao, Z., Lei, Y., & He, D. (2019). Early visual detection of wheat stripe rust using visible/near-infrared hyperspectral imaging. *Sensors*, *19*(4), 952. <https://doi.org/10.3390/s19040952>.
- Zhang, X., Han, L., Dong, Y., Shi, Y., Huang, W., Han, L., et al. (2019). A deep learning-based approach for automated yellow rust disease detection from high-resolution hyperspectral UAV images. *Remote Sensing*, *11*(13), 1554. <https://doi.org/10.3390/rs11131554>.
- Zhang, J., Huang, W., Li, J., Yang, G., Luo, J., Gu, X., et al. (2011). Development, evaluation and application of a spectral knowledge base to detect yellow rust in winter wheat. *Precision Agriculture*, *12*(5), 716–731. <https://doi.org/10.1007/s11119-010-9214-1>.
- Zheng, Q., Huang, W., Cui, X., Dong, Y., Shi, Y., Ma, H., et al. (2019). Identification of wheat yellow rust using optimal three-band spectral indices in different growth stages. *Sensors*. <https://doi.org/10.3390/s19010035>.
- Zheng, Q., Huang, W., Cui, X., Shi, Y., & Liu, L. (2018). New spectral index for detecting wheat yellow rust using sentinel-2 multispectral imagery. *Sensors*, *18*(3), 868. <https://doi.org/10.3390/s18030868>.

Publisher's Note Springer Nature remains neutral with regard to jurisdictional claims in published maps and institutional affiliations.

Affiliations

Ran Aharoni¹  · **Valentyna Klymiuk**^{2,3}  · **Benny Sarusi**^{1,4} · **Sierra Young**⁵  · **Tzion Fahima**^{2,3} · **Barak Fishbain**⁶ · **Shai Kendler**^{1,6}

¹ Department of Environmental Physics, Israel Institute for Biological Research, Ness-Ziona, Israel

² Institute of Evolution, University of Haifa, 199 Abba-Khushi Avenue, Mt. Carmel, 3498838 Haifa, Israel

³ Department of Evolutionary and Environmental Biology, University of Haifa, 199 Abba-Khushi Avenue, Mt. Carmel, 3498838 Haifa, Israel

⁴ Nuclear Research Center Negev, P.O.B 9001, 84190 Beer Sheva, Israel

⁵ Department of Biological and Agricultural Engineering, North Carolina State University, Weaver Laboratories, Campus Box 7625, Raleigh, NC 27695, USA

⁶ Faculty of Civil and Environmental Engineering, Technion – Israel Institute of Technology, 3200003 Haifa, Israel